A redox-active porous polymer based on poly(imide-triazine) as a high-performance cathode for lithium-ion batteries

Refka El Oueslati, Badr Jismy, Benjamin Flamme, Nicolas Leclerc, Fouad Ghamouss, Mohamed Abarbri

ARTICLE

Redox-Active Porous Polymer Based on Poly (Imides-Triazine) As High-Performance Cathode for Lithium-ion Batteries

Received 00th January 20xx,
Accepted 00th January 20xx

DOI: 10.1039/x0xx00000x

Refka El Oueslati,[a] Badr Jismy,*[a] Benjamin Flamme,[a] Nicolas Leclerc,[b] Fouad Ghamouss*[ac] and Mohamed Abarbri*[a]

Organic materials are gaining increasing interest as electrode materials for Lithium Ion Batteries (LIBs) due to their molecular diversity, high capacity, low cost, environmental friendliness and durability. However, most organic electrode materials suffer from poor electronic conductivity, limited active sites and high solubility in organic electrolytes, which impede their pratical use in LIB applications. To avoid these drawbacks, an insoluble redox-active porous polymer (RAPP) based on triazine and pyromellitic diimide has been prepared by a simple one-pot solvothermal polymerization and employed as a cathode material for LiBs. The Poly(Imide-Triazine) denoted as PIT, shows dual porosity combining micro and mesopores with a high specific surface area of about 674 $m^2 g^{-1}$ which facilitates the electrolyte penetration and ionic transportation and provides an interfacial Li storage allowing an additional capacity. Morever, the dual-redox active sites of C=N and C=O groups generate more capacity. Remarkably, the LiBs assembled with the synthesized PIT cathode show continuous activation with a high discharge capacity of 233 mAh g^{-1} after 300 cycles at 2 A g^{-1}. After an activation process, the PIT material delivers a very high discharge capacity (422 mAh g^{-1} at 0.5 A g^{-1}), excellent rate capabilities (268 mAh g^{-1} at 10 A g^{-1}) and extraordinary ultralong cycling stability keeping 65% of discharge capacity after 4000 cycles at 6 A g^{-1}. These unprecedented performances outperform most organic/polymeric cathode materials, making PIT a highly promising cathode material for LiBs for future electrochemical energy-storage applications.

Introduction

Nowadays, Lithium-ion battery (LIB) technology dominates the market as a common and important energy source for various consumer electronics and electric vehicles.[1] Commercial LIBs generally employ cathode materials, mainly based on inorganic lithium metal oxides, such as $LiMO_2$, LiM_2O_4, and $LiMPO_4$ (M = Co, Mn, Ni, etc.).[2] Nevertheless, these inorganic-based cathodes are in some cases expensive, scarce, hazardous, toxic, and/or environmentally unfriendly, leading to sustainability concerns.[3] In an attempt to overcome the issues of conventional inorganic materials, organic materials are attractive and candidate to be the next generation of LIBs cathodes due to their several inherent merits, such as wide structural diversity, high capacity, versatility of their properties, low cost, and good environmental compatibility.[4] Despite these interesting advantages, some organic electrode materials exhibit intrinsic weaknesses that severely limit their further commercial application, such as limited redox-active sites, thermal instability, low conductivity and more importantly, their high solubility in organic electrolytes. As a result, battery performance is relatively poor in terms of specific capacity, cyclability and rate performance.[4c,5] Consequently, several approaches have been proposed to tackle those issues, including the preparation of organic salts, the use of solid electrolyte, the polymerization of conjugated molecules with many redox-active sites, etc.[6] In this context, a new chemical approach that appears even more promising consists of embedding multi redox-active centers in an ordered two-dimensional or three-dimensional porous conjugated polymer, possessing highly cross-linked networks. Such a network is expected to allow easy and fast diffusion of ions (Li^+) through the pores, facilitating their access to the different redox-active sites and increasing the electronic conductivity, as well as addressing the solubility issue.[7] Therefore, redox-active Covalent Organic Frameworks (COFs), with uniform pore sizes and high surface areas, have recently emerged as very appealing electrode materials for various electrochemical-storage applications.[8] As a subclass of COFs, Covalent Triazine-based Frameworks (CTFs) have recently attracted tremendous attention owing to their excellent properties. Indeed, the electron-withdrawing triazine core in the CTFs is a rigid heteroaromatic ring that improves the physicochemical stability and increases the ability to accept Li-ions due to its high imine (C=N) content. In addition, the conjugated electrophilic triazine ring allows to tune the energy levels as well as the energy bandgap, and increases the materials conductivity.[9] Another class of organic materials has been widely investigated

[a] Laboratory of Physical-Chemistry of Materials and Electrolytes for Energy (PCM2E), University of Tours, 37200 Tours, France.
[b] ICPEES, UMR 7515, Université de Strasbourg, CNRS, 25 Rue Becquerel, 67087 Strasbourg Cedex 02, France.
[c] Department of Materials Science, Energy, and Nano-Engineering, Mohamed VI Polytechnic University, Ben Guerir 43150, Morocco.

† Footnotes relating to the title and/or authors should appear here.
Electronic Supplementary Information (ESI) available: [details of any supplementary information available should be included here]. See DOI: 10.1039/x0xx00000x

recently as cathode material in LIBs i.e. the imide-based polymers.[7d,10] Interestingly, their carbonyl (C=O) content leads to fast kinetics of charge/discharge cycles, high reversible capacity, excellent redox stability, and tunable redox potentials within the stability window of most lithium-ion electrolytes (0.75 to 4.3 V vs. Li/Li^+).[7d,10] Amazingly, there are very few reports on organic cathode materials containing both C=O and C=N groups as dual-redox active sites for LIB applications.[11] However, very high and appealing properties can be reached using a material with both functions, as shown by Jin et *al.*,[11a] who developed a 2D COF (BQ1-COF), composed of pyrazine and benzoquinone units. Indeed, with maximum accessible active sites (C=O and C=N) and minimal inactive groups, the BQ1-COF exhibits a reversible high capacity of 502.4 mAh g^{-1} at 0.05C. Likewise, Zhao et *al.*[11d] reported a novel COF cathode (TP-COF) with a dual-active-center (C=O on polyimide and C=N on triazine) and its exfoliated derivative (E-TP-COF). As a result, the pristine TP-COF showed a specific capacity of 25 mAh g^{-1} at a current density of 0.2 A g^{-1} and the exfoliated E-TP-COF delivered an initial capacity of more than 110 mAh g^{-1} at the same current density. The co-existence of both electroactive groups with a similar redox mechanism (C=N/C–N^- vs C=O/C–O^-) into one stable electrode material provides fast reaction kinetics and high specific capacities, as well as great versatility in the material design. These recent works lead to a better understanding of structure-property relationships and discover new high electrochemical performance of battery materials. Inspired by the above examples, we propose in this work, to use a dual-active-center (C=O and C=N) COF, named Poly(Imides-Triazine) (PIT), as organic cathode material for LIBs. This COF, combining pyromellitic diimide and triazine units, has already been used in various applications, including gas storage, photocatalysis and biomolecules adsorption.[12] However, its application in the field of energy storage and conversion has never been investigated to date. For this purpose, we demonstrate that PIT can also successfully be used as cathode material, leading to superior electrochemical performances in LIB devices. Prepared by a simple one-pot solvothermal polymerization, our PIT COF exhibits exceptionnally high physico-chemical stability, a specific BET surface area of about 674 m^2 g^{-1} that provides interfacial Li storage with abundant active sites and hierarchical porous structure that is beneficial for the fast transport of electrons and ions. After an activation process, the assembled batteries based on PIT cathode material exhibit a very high reversible discharge capacity (422 mAh g^{-1} at 0.5 A g^{-1}), an excellent rate capability (268 mAh g^{-1} at 10 A g^{-1}) and an extraordinary ultralong cycling stability, keeping 65% of discharge capacity after 4000 cycles at 6 A.g^{-1}. These unprecedented performances, outperforming most organic/polymeric materials, combined with a simple and low-cost synthesis, can achieve multi-aspect improvement to accelerate the application of COFs for next-generation energy storage devices.

Results and discussion

In the literature, two different routes have been reported to synthesize the poly(Imide-Triazine) (PIT) COF. The first one simply involves a solid-state thermal condensation of the melamine (MA) and the pyromellitic dianhydride (PMDA) at high temperature (286°C, corresponding to the PMDA melting temperature). PITs synthesized following this route exhibit high crystallinity and small specific surface area.[12a–l] The second route involves a solvothermal method using DMSO as solvent at 180°C. This approach produces amorphous PITs with large specific surface area and high porosity.[12m–q] Therefore, we selected this latter synthetic route to elaborate our PIT COF (**Scheme 1**). The use of dry DMSO is highly recommended to reach a larger specific surface area and porosity. Due to their extended backbone and high molecular weight, the PIT material is not soluble enough in most common organic solvents which limits the chemical characterization to Fourier transform infrared (FTIR) spectroscopy.

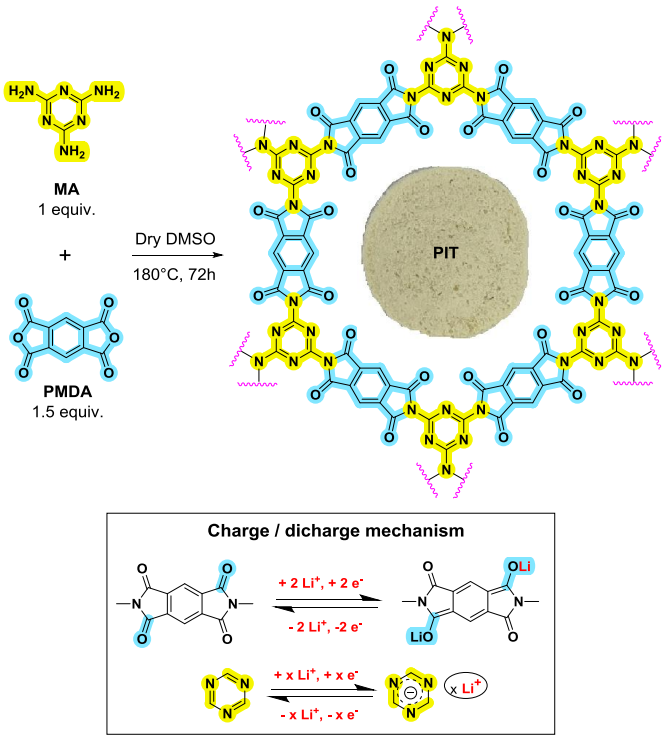

Scheme 1 Schematic illustration of the one-pot synthetic route for Poly (Imide-Triazine) (PIT) and proposed energy storage process.

Accordingly, the result of the polycondensation between PMDA and melamine was analyzed by FTIR spectroscopy as displayed in Fig. 1a. PMDA shows two bands at 1860 and 1230 cm^{-1} originating from the anhydride groups. Stretching and bending vibrations for the $-NH_2$ group in MA, can be seen at 3600–3100 and 1025 cm^{-1}. In the FTIR spectrum of PIT, the stretch vibration of $-NH_2$ (MA) and –C=O (PMDA) disappear, while new peaks are clearly visible at 1792 and 1726 cm^{-1} (see zoom in PIT FTIR curve). They are attributed to asymmetric and symmetric stretching of the C=O groups on the five-membered imide rings. A new band at 1360 cm^{-1} can be assigned to the stretching vibration of C–N–C as produced by the reaction of an anhydride and an amine. Other peaks around 1534 and 1459 cm^{-1} are attributed to quadrant and semicircle stretching of triazine rings. These infrared results are very consistent with previously reported data.[12m–q] All this indicates that our polycondensation has indeed taken place successfully. Furthermore, the expected chemical composition (C, H, N, and O) of the PIT was also supported by elemental analysis. Thus, the

synthesized PIT contains 38.42 wt% carbon, 5.42 wt% hydrogen and 33.76 wt% nitrogen, which were close to the theoretical values of 54.15 wt% carbon, 0.76 wt% hydrogen and 21.05 wt% nitrogen. It is worth noting that the elemental analysis showed a few differences between experimental and calculated results, and the observed deviation is probably due to the formation of phthalimide derivatives. The previously reported elemental analysis results of PIT and more details relative to the theorical composition are provided in Table S1. These results are in good agreement with the previously reported analysis, which proved the formation of PIT.[12m]

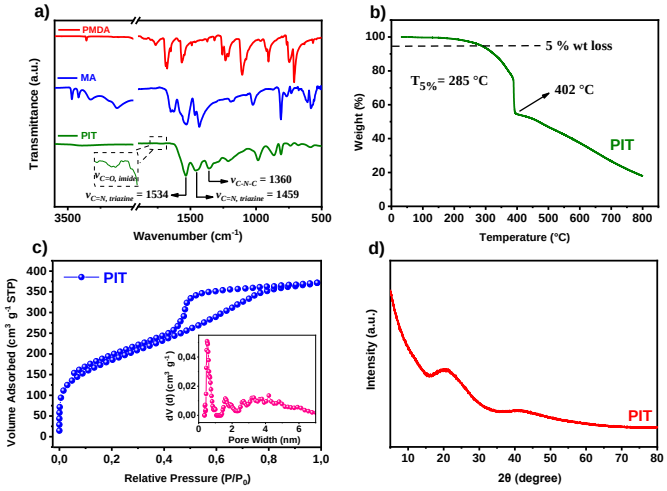

Fig. 1 (a) FT-IR spectra of PIT. (b) TGA curves of PIT under nitrogen atmosphere at a heating rate of 10 °C min^{-1}. (c) N_2 adsorption-desorption isotherms of PIT at 77K with pore-size distribution profile calculated using the NLDFT method. (d) XRD patterns of PIT.

In order to assess the thermostability of the PIT, thermogravimetric analysis (TGA) for PIT was carried out under nitrogen atmosphere (Fig. 1b). The TGA profile of PIT shows thermal degradation temperatures at 5% weight loss ($T_{5\%}$) in 285 °C, a weight loss of 40% in the region of 215–402 °C and residue remaining at 800 °C, suggesting a good thermal stability of PIT. The higher thermal stability of our PIT is also in good agreement with those reported in previous studies.[12m–q] The BET specific surface areas (S_{BET}), total pore volumes (V_{total}), and pore size diameters of the PIT COF were measured through nitrogen adsorption–desorption isotherms analysis collected at 77 K (Figure 1c). The porosity properties are listed and compared to previously reported results in Table S2. As shown in Figure 1c, the values of S_{BET}, V_{total} and V_{micro} for our PIT were 674 m^2 g^{-1}, 0.543 and 0.267 cm^3 g^{-1}, respectively. The dominant peaks centered at 0.5 and 1.6 nm, indicate the presence of a microporous architecture. In addition, other several small peaks distributed between 2- and 7 nm, revealing the presence of a mesoporous structure. As a result, the BET isotherm of PIT has been classified as type IV, according to the IUPAC classification. The value of V_{meso}, determined by $V_{total} - V_{micro}$, was 0.276 cm^3 g^{-1}. Our PIT-COF exhibits a ratio of mesopore volume (V_{meso} /V_{total}) value of 51%, reflecting the micropores-mesopores texture of PIT networks. This result was also proved by the pore size distribution curve (inset in Fig. 1c) based on the non-local density function theory (NL-DFT) method. The obtained PIT sample exhibits a significantly higher BET specific surface area and a different pore size distribution than other samples prepared by the same solvothermal method reported in the literature (Table S2),[12m] which might be attributed to the use of anhydrous DMSO during polymerization. Indeed, the use of dry DMSO avoids the hydrolysis of DMAP into their corresponding carboxylic acid. The high BET specific surface area and the large pore volume of PIT provide high accessibly to the redox active sites. To further identify the crystalline structure of the PIT, the powder X-ray diffraction (PXRD) analysis was carried out (Fig. 1d). Only a broad diffraction peak can be observed at about 25°, which indicates the amorphous nature of our PIT. The XRD pattern of the PIT is in good agreement with those reported in the literature using the solvothermal method,[12m–q] and clearly different from the crystalline ones obtained by solid-state thermal condensation (Table S3).[12m–q] The morphology of the PIT characterized by scanning electron microscopy (SEM) reveals a compact morphology with a typical hierarchical porous architecture (Fig. 2), which is consistent with the BET analysis results (Fig. 1c,d).

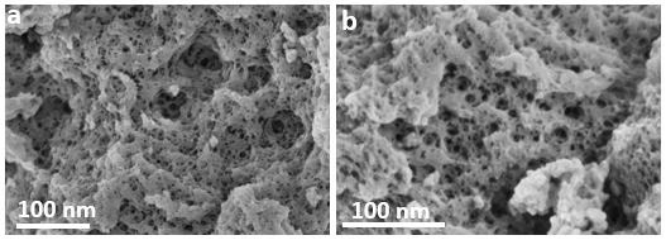

Fig. 2 Microscopic Characterization of PIT framework. (a and b) SEM pictures of PIT.

All the above characterizations are in good agreement with literature results when a similar synthesis route was used (Table S3).

The structural stability of the cathode material was studied by testing their solubility *ex*-situ in the electrolyte (Fig. 3a). Immersion of the PIT in a 1:1 vol DOL/ DME mixture (solvent used in battery electrolytes) for different soaking times shows no dissolution as confirmed by FTIR spectroscopy (Fig. 3b). The excellent chemical stability of the PIT framework results from the rigid pyromellitic diimide and triazine (C_3N_3) units, including strong C=C and C=N bonds. This stability in the electrolyte is very promising for application in high-performance LIBs.

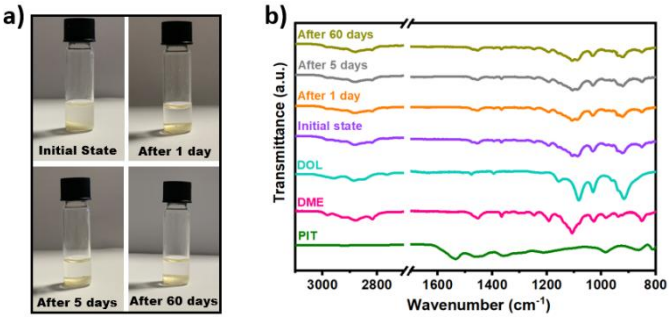

Fig. 3 (a) Pictures illustrating the PIT immersed in the electrolyte of LIBs for different soaking time: pristine, and after 1, 5 and 60 days, respectively. (b)

FT-IR spectra of the electrolyte supernatant after different soaking time. The absence of PIT signatures within the supernatants demonstrates its insolubility in the electrolyte.

The electrochemical properties of the PIT were then investigated by preparing the working electrode using super-P, and PVDF as described in the experimental part. The working electrode was assembled in CR2032-type coin cells with lithium metal foil as reference/counter electrode, a GF/C type Whatmans separator, and 1 M LiTFSI in a DOL: DME mixture (v : v = 1 : 1) electrolytes inside an argon-filled glovebox. PIT was first tested as an active cathode material in the high potential window of 1.3–3.6 V (*vs* Li/Li$^+$). The long-term cycling performance of PIT at a high current density of 2 A g^{-1} was evaluated and is shown in Fig. 4a.

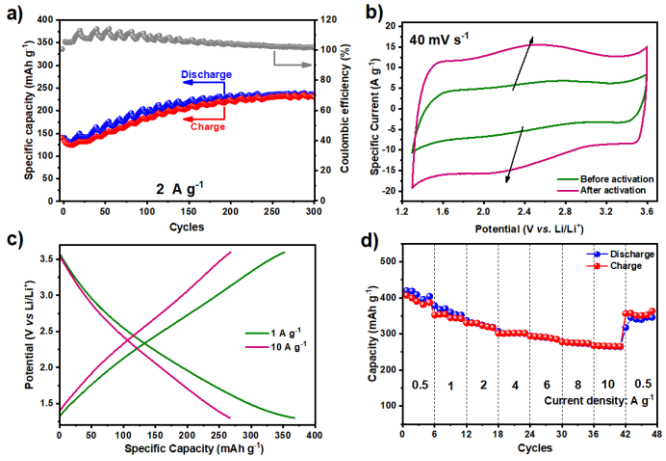

Fig. 4 Electrochemical performance of PIT electrodes. (a) Cycling performance of the PIT at current densities of 2 A g^{-1}. (b) CV curve of the PIT electrode at a scan rate of 40 mV s^{-1} before and after activation. (c) Charge – discharge profiles of PIT at 1 and 10 A g^{-1}. (d) Rate capacity of the PIT at various current densities from 0.5 to 10 A g^{-1}.

The capacity contribution of current collector (Carbon paper) is negligible (Fig. S2), while the one of the conductive additive (super P) is less than 50 mAh g^{-1} (Fig. S3). Discharge capacity decreased during the first 10 cycles to ≈140 mAh g^{-1} due to low electronic conductivity of organic electrode materials, then increased to ≈233 mAh g^{-1} after 300 cycles. This progressive capacity increase with cycling is the activation process may be due to the gradual exposure of PIT-COF active sites to the electrolyte. This phenomenon has been reported for many organic electrode materials.[13] However, we have identified an electrochemical oscillation phenomenon during charge/discharge, which could be due to the fast increase in capacity during the activation process.[13d] This activation process can be clearly observed by cyclic voltammetry (CV) measurements (Fig. 4b) with an overall specific current increase after activation. In addition, the CV conducted at ambient temperature in the potential window of 1.3−3.6 V (*vs* Li/Li$^+$) at a scan rate of 40 mV s^{-1} demonstrates that the PIT-COF displayed a broad reversible peak indicating its sensitivity to redox (pseudocapacitive) processes. The cathodic scan of PIT exhibits an oxidation peak at ∼2.4 V, which can be ascribed to the insertion of Li$^+$ into the carbonyl groups in pyromellitic diimide ring. In reverse scan, a broader anodic reduction peak located at ∼2.2 V is observed, corresponding to the reversible delithiation process.[11d,14-16] The presence of redox-active units within the PIT suggests that the mechanism for Li+ storage is not purely capacitive. The galvanostatic charge/discharge (GCD) profiles of PIT (Fig. 4c) evaluated in the same potential window, reveal a very high capacity of 367 and 268 mAh g^{-1} at current densities of 1 and 10 A g^{-1}, respectively. It is worth noting that such values are among the highest ones reported nowadays for cathodes using triazine and/or pyromellitic diimide-based COFs (Table S4).[11d,11f,14-17] The discharge capacity is always lower than their theoretical capacity, giving coulombic efficiency of 94% for 377 mAh g^{-1} and 70% for 268 mAh g^{-1} of their theoretical capacity (400 mAh g^{-1}, calculated according to three-electron redox mechanism per triazine unit and two-electron redox mechanism per diimide centers) (SI).

Rate capability performance is another key requirement for the development of high-performance organic cathode materials for application in LIBs. Fig. 4d shows the rate capability of the PIT cathode at different current densities from 0.5 to 10 A g^{-1} in the voltage range of 1.3–3.6 V. Importantly, it can be found that specific capacity is not strongly dependent on the current density. After the activation process at 2 A g^{-1}, PIT displayed a reversible capacity decrease from 422 to 268 mAh g^{-1} when the current density increases from 0.5 to 10 A g^{-1}, surpassing most conventional cathodes, such as LFP or LCO, as well as most organic/polymeric LIB cathodes ever reported (Table 1). More importantly, when the current density was reversed back to 0.5 A g^{-1}, the PIT electrode almost recovers its initial specific capacity, indicating the excellent structural stability of the PIT-COF backbone during the electrochemical reactions. The high rate capacity under high current density conditions is attributed in part to the higher porosity, which provide better electrolyte penetration and fast transport of Li-ions and electrons. The unique structure of PIT with micro/mesopores and high specific surface area make the PIT a suitable Li-ion storage material even at high charge/discharge rates.

As determined by the electrochemical impedance spectroscopy (EIS) results (Fig. 5a), the charge-transfer resistance (Rct) of PIT cathode decreased from 56 Ω before cycling to 22 Ω after 100 cycles, and 9 Ω after 300 cycles.

This interfacial resistance decrease can be correlated to the charge transport kinetics, explaining the gradual activation process during cycling. Figures 5b and 5c show the long-term cyclability of PIT electrodes at a high current density of 6 A g^{-1}. Remarkably, the initial discharge capacity reaches 288 mAh g^{-1} and retains a reversible capacity of 187 mAh g^{-1} after 4000 cycles, corresponding to a high-capacity retention of 65%. Moreover, the coulombic efficiency is close to 100% during the whole cycling process.

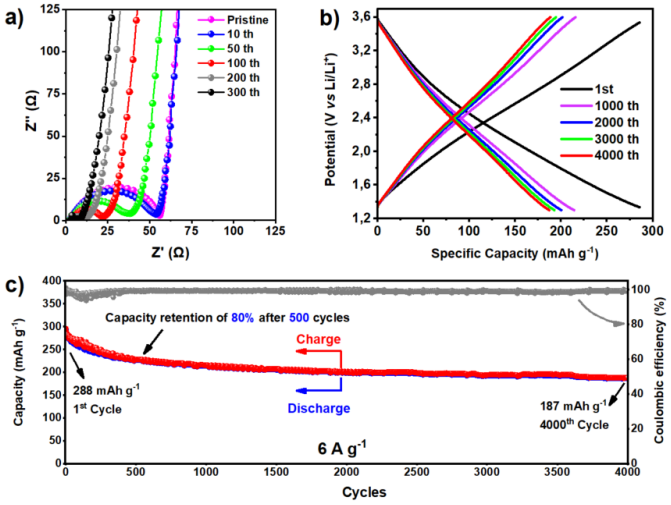

Fig. 5 Electrochemical performance of PIT electrodes. (a) Nyquist plots of PIT before and after the 10th, 50th, 100th, 200th and 300th cycles under a current density of 2 A g^{-1}. (b) Charge/discharge curves of different cycles of PIT at a current density of 6 A g^{-1}. (c) Long-term cycling stability of the PIT at a current density of 6 A g^{-1}

To further understand the fast rate capability of PIT cathode, the electrochemical reaction kinetics was investigated by collecting a series of CV curves in the potential range of 1.3–3.6 V at different scan rate from 5 to 60 mV s^{-1} (Fig. 6).

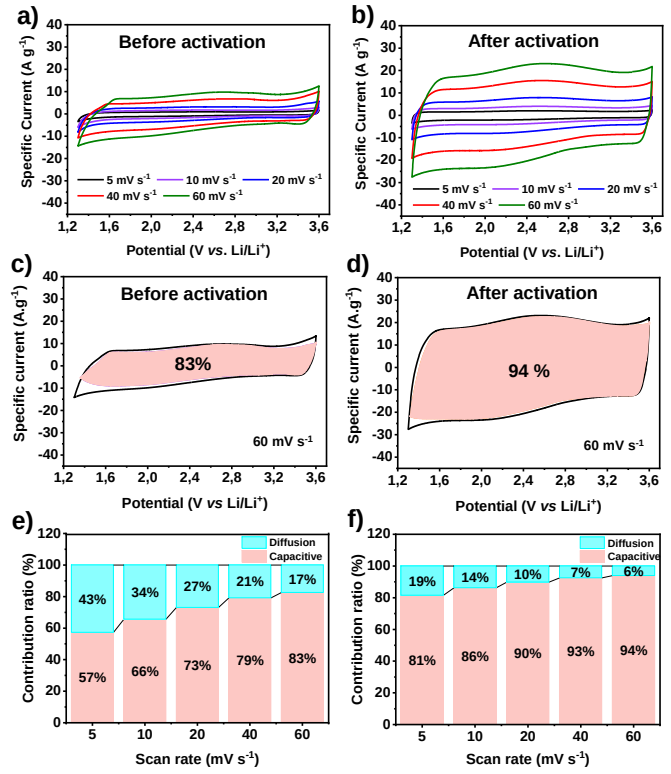

Fig. 6 Kinetic analysis of the PIT framework. (a) Cyclic voltammograms at various scan rates from 5 to 60 mV s^{-1} before and (B) after activation. (c) Capacitive contributions at a scan rate of 60 mV s^{-1} before activation and (d) after activation. (e) The pseudocapacitive and diffusion-controlled charge storage contributions at different scan rates before and (f) after activation.

The quantitative contribution of diffusion and surface-controlled processes at different scan rates were calculated according to the following equation:

$$i\,(V) = k_1 v + k_2 v^{1/2}$$

where i is the total current, v is the scan rate, k_1 and k_2 are constants, $k_1 v$ and $k_2 v^{1/2}$ represent the pseudocapacitive and the diffusion-controlled contribution, respectively. Furthermore, k_1 and k_2 can be determined by plotting $iv^{-1/2}$ versus $v^{1/2}$ for the linear simulation.[18] As shown in Fig. 6**,** the capacitive contributions increase with the increasing scan rate and with the activation process. They range from 57 to 83 % before activation and from 81 to 94% after activation, confirming the kinetically fast pseudocapacitive process. The high BET surface area with abundant redox active units (C=N and C=O) may plays a key role in the highly capacitive contribution of PIT, which is highly beneficial for the high rate performance of LIBs.

The Ragone plot in Fig. 7a shows that the PIT electrode, as compared to recently reported organic LIBs, exhibits higher energy density (648 Wh kg^{-1}) at high power density (24.5 KW kg^{-1}). We then used the PIT/Li coin cell battery to power up a light-emitting diode (LED) array to examine its power ability for potential practical applications. As shown in Fig. 7b, our PIT-COF could easily lighten the array, constructed with 28 red LEDs and 36 yellow LEDs.

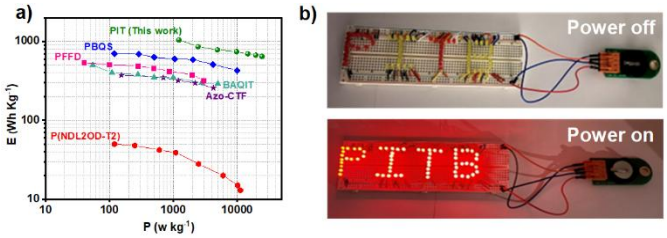

Fig. 7 (a) Ragone plots for a Lithium-organic energy storage device using, PIT, PBQS,[19] PFFD,[20] BAQIT,[21] Azo-CTF[17] and NDL2OD-T2[22] (b) Pictures showing the PIT//Li coin cell illuminating 64 commercialized red LEDs.

Experimental

***General information*:** All reagents commercially available were of analytical grade and used as received without any purification or treatment. The anydrous Liquid reagents such as Dimethyl sulfoxide (DSMO), *N*-methyl-2-pyrrolidinone (NMP), 1,3-Dioxolane (DOL, 99.8%) and 1,2-Dimethoxyethane (DME, 99.5%) were purchased from Sigma Aldrich. Bis(trifluoromethane)sulfonimide lithium salt (LiTFSI, 99%) was purchased from Fluorochem. Poly(vinylidene fluoride) (PVDF), Melamine (MA), Pyromellitic dianhydride (PMDA) and pure lithium foil (thickness 0.38 mm, 99.9%) were obtained from Sigma Aldrich. Carbon paper (Sigracet 25 BC, SGL Carbon) was supplied by fuel cell store, USA.

***Material Synthesis*:** The Poly(Imide-Triazine) was synthesized following (according) a slightly modified solvothermal method (procedure) adopted from the literature (Scheme 1). An oven-dried 500 mL round-bottom flask equipped with a stir bar was charged with pyromellitic dianhydride (23 g, 0.105 mol) and dry DMSO. The reaction mixture was cooled to 0 °C before careful addition of melamine (8.82 g, 0.07 mol). The resulting solution was stirred for

30 min at room temperature then heated to 180°C under Argon atmosphere for 72 h. After cooling to room temperature, the resulting PIT precipitate was collected by filtration and then washed several times with DMSO, distilled water, ethanol, methanol, tetrahydrofuran and diethyl ether, respectively. The filtred PIT was then dried under vacuum at 100°C for 12 hours to give a white powder in 72% (40.8 g) yield. The final polymer was insoluble in organic solvents. Elemental analysis calculated for $C_{18}H_3N_6O_6$: C, 54.15; H, 0.76; N, 21.05; O, 24.04%. Found: C, 38.42; H, 5.42; N, 33.76%.

***Materials characterization*:** The Fourier transform infrared spectrometry (FTIR) was performed on a spectrum TWO (PerkinElmer). Elemental analysis was determined by the Service d'Analyses–Chromato-Masse (BioCIS, UMR 8076, Paris, France) using an elemental analyzer (CHNS Vario Micro cube ELEMENTAR). The porosity and surface area of PIT are investigated using a Automated Surface Area and Pore Size Analyzer (QUADRASORB evo). PIT morphology was evaluated by Scanning Electron Microscopy (SEM) recorded on a ZEISS ULTRA Plus (Oberkochen, Germany). EDS were performed out using a Silicon Drift Detector (SDD) detector. Thermostability of samples was inspected by thermogravimetric analyses (TGA) on a STA 6000 (PerkinElmer) within the temperature range of 30–800°C at a heating rate of 10°C min^{-1} under a nitrogen atmosphere. X-Ray Diffraction (XRD) measurements was recorded on a D8 Bruker diffractometer using Cu Kα (λ = 1.5418 Å) radiation in the 2θ range of 5°– 80.

***Battery Fabrication and Electrochemical Measurement*:** Cathode electrode was prepared by mixing 50 wt % active material (PIT-COF), 40 wt % conductive carbon black (carbon black, Super P), and 10 wt % binder (PVDF). The active materials (PIT) powder was manually milled in an agate mortar with conductive carbon black for 30 min. A solution of PVDF in NMP (1.5 mL) was then added to generate a slurry. After stirring for 12 h at room temperature a finely dispersed viscous slurry was obtained, and this was painted with a fine brush on conductive carbon paper (diameter of 14 mm). The ''wet'' electrode was further dried at 50°C for 4h in oven to partially remove the NMP, followed by drying under vacuum pressure in a glass oven (BÜCHI B-585) at 80°C for 12h. Finally, the dry electrodes were transferred directly into an argon-filled glovebox with both oxygen and moisture contents below 1 ppm. The substrates were weighed on a Sartorius MSA 66.5-000-DM balance with an accuracy of ± 0.001 mg. The loading density of the active materials (PIT) is uniform and about 0.5 mg cm^{-2}. Coin cells (CR2032) were then assembled using pure lithium foil (thickness of 0.6 mm) as the counter electrode and glass microfiber filters (Whatman GF/C, diameters of 16 mm) as the separator. In addition, a mixture of DOL and DME (1 :1 v/v) containing 1.0 M LiTFSI was used as the electrolyte. The added amount of the electrolyte in a single buttom cell is about 100 µL. It is important to note that this whole process was carried out inside the argon-filled glovebox. The coin cells were kept at room temperature for 12 h before the galvanostatic charge/discharge cycling. Then, it was placed in CR2032 coin cell holders (Origalys Electrochem) and an electrochemical characterization was carried out using a Biologic BCS-810 and VMP3 battery cycler. Each cell was repeated several times to ensure reproducibility of results. Cut-off voltages for cyclic voltammetry and galvanostatic cycling tests were 1.3-3.6 V (*vs* Li/Li^+). Electrochemical Impedance Spectroscopy (EIS) experiments were performed using the CR2032-type coin cells before and after different charge/discharge cycles and the measurements were performed over the frequency ranges from 1.0 MHz to 10 mHz, with an applied amplitude of 10 mV. The currents and the specific capacity were calculated according to the weight of the active material in the electrode. All of the electrochemical tests were evaluated at room temperature.

Conclusions

We have successfully synthesized a covalent based poly(imides-Triazine) framework *via* the solvothermal method and used as an organic cathode material for LIBs. The unique PIT-COF structure with large surface area, porous structure, and abundance redox-active sites provide exceptional electrochemical performances. Thus, the PIT-based cathode provided an initial high reversible capacity output of 422 mAh g^{-1} at a current density of 0.5 A g^{-1} and retained a reversible capacity of 187 mAh g^{-1} at 6 A g^{-1} for 4000 cycles. Additionally, the PIT network exhibited an ultra-high power density of 24.5 kW kg^{-1} and maintained a high energy density of 648 W h kg^{-1}. Benefiting from its porous structure, the PIT framework exhibited a dominant pseudo-capacitive behavior. This work may offer some new guidelines for the development of organic electrodes for high-energy and high-power energy storage devices.

Author Contributions

Refka El Oueslati: conceptualization, data curation, methodology, writing – original draft. Badr Jismy: conceptualization, data curation, methodology, supervision, writing – original draft, writing – review and editing. Benjamin Flamme: methodology, validation, writing – review and editing. Niolas Leclerc: validation, writing – review and editing. Fouad Ghamouss: supervision, validation, funding acquisition, project administration, writing – review and editing. Mohamed Abarbri: supervision, validation, funding acquisition, project administration, writing – review and editing.

Conflicts of interest

The authors declare no conflict of interest.

Acknowledgements

The authors would like to thank “La Région Centre Val de Loire” for financial support, Pierre Ivan Raynal for his help in SEM and EDS acquisitions and Cecile Autret-Lambert for XRD analysis.

Notes and references

1 (a) X. Zeng, M. Li, D. Abd El-Hady, W. Alshitari, A. S. Al-Bogami, J. Lu, K. Amine, *Adv. Energy Mater.*, 2019, **9**, 1900161; (b) Y. Lu, J. Chen, *Nat. Rev. Chem.*, 2020, **4**, 127–142; (c) F. M. N. U. Khan, M. G. Rasul, A. S. M. Sayem, N. K. Mandal, *J. Energy Storage*, 2023, **71**, 108033; (d) D. L. Thompson, J. M. Hartley, S. M. Lambert, M. Shiref, G. D. J. Harper, E. Kendrick, P. Anderson, K. S. Ryder, L. Gaines, A. P. Abbott, *Green Chem.*, 2020, **22**, 7585–7603; (e) V. Ruiz, A. Pfrang, A. Kriston, N. Omar, P. Van den Bossche, L. Boon-Brett, *Renew. Sust. Energ. Rev.*, 2018, **81**, 1427–1452.

2 (a) G.-L. Xu, X. Liu, A. Daali, R. Amine, Z. Chen, K. Amine, *Adv. Funct. Mater.*, 2020, **30**, 2004748; (b) C. Tian, F. Lin, M. M. Doeff, *Acc. Chem. Res.*, 2018, **51**, 89−96; (c) S. Kim, G. Park, S. J. Lee, S. Seo, K. Ryu, C. H. Kim, J. W, Cho, *Adv. Mater.*, 2023, **35**, 2206625.

3 (a) D. Larcher, J-M. Tarascon, *Nat. Chem.*, 2015, **7**, 19–29; (b) K. Du, E. H. Ang, X. Wu, Y. Liu, *Energy Environ. Mater.*, 2022, **5**, 1012–1036; (c) B. E. Murdock, K. E. Toghill, N. Tapia-Ruiz, *Adv. Energy Mater.*, 2021, **11**, 2102028.

4 (a) B. Esser, F. Dolhem, M. Becuwe, P. Poizot, A. Vlad, D. Brandell, *J. Power Sources*, 2021, **482**, 228814; (b) Y. Wu, R. Zeng, J. Nan, D. Shu, Y. Qiu, S.-L. Chou, *Adv. Energy Mater.*, 2017, **7**, 1700278; (c) S. Lee, G. Kwon, K. Ku, K. Yoon, S.-K. Jung, H.-D. Lim, K. Kang, *Adv. Mater.*, 2018, **30**, 1704682; (d) T. Kim, W. Song, D.-Y. Son, L. K. Ono, Y. Qi, *J. Mater. Chem. A*, 2019, **7**, 2942–2964.

5 (a) Q. Zhao, Y. Lu, J. Chen, *Adv. Energy Mater.*, 2017, **7**, 1601792; (b) Y. Lu, Q. Zhang, L. Li, Z. Niu, J. Chen, *Chem.*, 2018, **4**, 2786–2813.

6 (a) J. Heiska, M. Nisula, M. Karppinen, *J. Mater. Chem. A*, 2019, **7**, 18735–18758; (b) M. Li, R. P. Hicks, Z. Chen, C. Luo, J. Guo, C. Wang, Y. Xu, *Chem. Rev.*, 2023, **123**, 1712−1773; (c) Q. Zhao, C. Guo, Y. Lu, L. Liu, J. Liang, J. Chen, *Ind. Eng. Chem. Res.*, 2016, **55**, 5795−5804.

7 (a) B. Zhang, W. Wang, L. Liang, Z. Xu, X. Li, S. Qiao, *Coord. Chem. Rev.*, 2021, **436**, 213782; (b) K. Amin, N. Ashraf, L. Mao, C. F. J. Faul, Z. Wei, *Nano Energy*, 2021, **85**, 105958; (c) D. Luo, M. Li, Q. Ma, G. Wen, H. Dou, B. Ren, Y. Liu, X. Wang, L. Shui, Z. Chen, *Chem. Soc. Rev.*, 2022, **51**, 2917–2938; (d) H. Wang, C.-J. Yao, H.-J. Nie, K.-Z. Wang, Y.-W. Zhong, P. Chen, S. Mei, Q. Zhang, *J. Mater. Chem. A*, 2020, **8**, 11906–11922.

8 (a) T. Sun, J. Xie, W. Guo, D.-S. Li, Q. Zhang, *Adv. Energy Mater.*, 2020, **10**, 1904199; (b) M. Wu, Y. Zhao, B. Sun, Z. Sun, C. Li, Y. Han, L. Xu, Z. Ge, Y. Ren, M. Zhang, Q. Zhang, Y. Lu, W. Wang, Y. Ma, Y. Chen, *Nano Energy*, 2020, **70**, 104498; (C) L. Kong, M. Liu, H. Huang, Y. Xu, X.-H. Bu, *Adv. Energy Mater.*, 2022, **12**, 2100172.

9 (a) P. Xiong, S. Zhang, R. Wang, L. Zhang, Q. Ma, X. Ren, Y. Gao, Z. Wang, Z. Guo, C. Zhang, *Energy Environ. Sci.*, 2023, **16**, 3181–3213; (b) Y. Zheng, N. A. Khan, X. Ni, K. A. I. Zhang, Y. Shen, N. Huang, X. Y. Kong, L. Ye, *Chem. Commun.*, 2023, **59**, 6314–6334.

10 (a) A. Nimkar, G. Bergman, E. Ballas, N. Tubul, N. Levi, F. Malchik, I. Kukurayeve, M. S. Chae, D. Sharon, M. Levi, N. Shpigel, G. Wang, D. Aurbach, *Angew. Chem. Int. Ed.*, 2023, 62, e202306904; (b) Q. Zhang, Y. Dou, Q. He, S. Deng, Q. Huang, S. Huang, Y. Yang, *Energy Environ. Mater.*, 2022, **5**, 1037–1059.

11 (a) Z. Jin, Q. Cheng, A. M. Evans, J. Gray, R. Zhang, S. T. Bao, F. Wei, L. Venkataraman, Y. Yang, C. Nuckolls, *Chem. Sci.*, 2022, **13**, 3533–3538; (b) D.-H. Yang, Z.-Q. Yao, D. Wu, Y.-H. Zhang, Z. Zhou, X.-H. Bu, *J. Mater. Chem. A*, 2016, **4**, 18621–18627; (c) X. Liu, Y. Jin, H. Wang, X. Yang, P. Zhang, K. Wang, J. Jiang, *Adv. Mater.*, 2022, **34**, 2203605; (d) G. Zhao, H. Li, Z. Gao, L. Xu, Z. Mei, S. Cai, T. Liu, X. Yang, H. Guo, X. Sun, *Adv. Funct. Mater.*, 2021, **31**, 2101019; (e) M. Wu, Y. Zhao, B. Sun, Z. Sun, C. Li, Y. Han, L. Xu, Z. Ge, Y. Ren, M. Zhang, Q. Zhang, Y. Lu, W. Wang, Y. Ma, Y. Chen, *Nano Energy*, 2020, **70**, 104498; (f) K. Li, Y. Wang, B. Gao, X. Lv, Z. Si, H.-G. Wang, *J. Colloid Interface Sci.*, 2021, **601**, 446–453.

12 (a) S. Chu, Y. Wanga, C. Wanga, J. Yang, Z. Zou, *Int. J. Hydrogen Energy*, 2013, **38**, 10768–10772; (b) P. Meng, J. Huang, X. Liu, *Appl. Surf. Sci.*, 2019, **465**, 125–135; (c) R. Pan, J. Wu, W. Wang, C. Cheng, X. Liu, *Colloids Surf. A: Physicochem. Eng. Asp.*, 2021, **621**, 126511; (d) C. Ma, H. Zhu, J. Zhou, Z. Cui, T. Liu, Y. Wang, Y. Wang, Z. Zou, *Dalton Trans.*, 2017, **46**, 3877–3886; (e) V. A. Kuehl, M. J. Wenzel, B. A. Parkinson, L. S. Oliveira, J. O. Hoberg, *J. Mater. Chem. A*, 2021, **9**, 15301–15309; (f) Y. Zhang, M.-S. Zhang, Y. Zhang, X.-W. Chen, J.-H. Wang, *RSC Adv.*, 2016, **6**, 46002–46007; (g) T. Wang, R. Xue, H. Chen, P. Shi, X. Lei, Y. Wei, H. Guo and W. Yang, *New J. Chem.*, 2017, **41**, 14272–14278; (h) S. Chu, Y. Wang, Y. Guo, P. Zhou, H. Yu, L. Luo, F. Kong and Z. Zou, *J. Mater. Chem.*, 2012, **22**, 15519–15521; (i) L. Lin, P. Ye, C. Cao, Q. Jin, G.-S. Xu, Y.-H. Shen and Y.-P. Yuan, *J. Mater. Chem. A*, 2015, **3**, 10205–10208; (j) J. Yang, S. Chu, Y. Guo, L. Luo, F. Kong, Y. Wang and Z. Zou, *Chem. Commun.*, 2012, **48**, 3533–3535; (k) J.-Y. Li, X. Jiang, L. Lin, J.-J. Zhou, G.-S. Xu and Y.-P. Yuan, *J. Mol. Catal. Chem.*, 2015, **406**, 46–50; (l) J.-D. Xiao, L.-G. Qiu, Y.-P. Yuan, X. Jiang, A.-J. Xie, Y.-H. Shen, *Inorg. Chem. Commun.*, 2013, **29**, 128–130; (m) Y. Luo, B. Li, L. Liang, B. Tan, *Chem. Commun.*, 2011, **47**, 7704; (n) H. Zhu, C. Wang, J. Zhou, M. Wan, Y. Wang, Z. Zou, M. Terrones, *J. Porous Mater.*, 2018, **25**, 1659-1668; (o) J. Zhou, Y. Wang, X. Hao, C. Ma, Y. Wang, Z. Zou, *J. Phys. Chem. C*, 2018, **122**, 1037−1043; (p) S. Chu, Y. Hu, J. Zhang, Z. Cui, J. Shi, Y. Wang, Z. Zou, *Int. J. Hydrogen Energy*, 2021, **46**, 9064–9076; (q) Y. Wang, Q. Gao, Q. You, G. Liao, H. Xia, D. Wang, *React. Funct. Polym.*, 2016, **103**, 9–16.

13 (a) J. Ryu, B. Park, J. Kang, D. Hong, S.-D. Kim, J.-K. Yoo, J. W. Yi, S. Park, Y. Oh, *ACS Nano*, 2019, **13**, 14357−14367; (b) H. Zhao, H. Chen, C. Xu, Z. Li, B. Ding, H. Dou, X. Zhang, *ACS Appl. Energy Mater.*, 2021, **4**, 11377–11385; (c) Z. D. Lei, Q. S. Yang, Y. Xu, S. Y. Guo, W. W. Sun, H. Liu, L. P. Lv, Y. Zhang, Y. Wang, *Nat. Commun.*, 2018, **9**, 576; (d) Z. Zhang, Y. Zhou, P. Chen, S. Zeng, W. Nie, Y. Xu, *ACS Appl. Energy Mater.*, 2021, **4**, 12882-12891; (e) F. Jiang, Y. Wang, T. Qiu, Y. Zhang, W. Zhu, C. Yang, J. Huang, Z. Fang, G. Dai, *ACS Appl. Mater. Interfaces*, 2021, **13**, 48818−48827; (f) O. Buyukcakir, J. Ryu, S. H. Joo, J. Kang, R. Yuksel, J. Lee, Y. Jiang, S. Choi, S. H. Lee, S. K. Kwak, S. Park, R. S. Ruoff, *Adv. Funct. Mater.*, 2020, **30**, 2003761; (g) T. Sun, Z.-J. Li, Y.-F. Zhi, Y.-J. Huang, H. J. Fan, Q. Zhang, *Adv. Funct. Mater.*, 2021, **31**, 2010049; (h) L. Zhai, G. Li, X. Yang, S. Park, D. Han, L. Mi, Y. Wang, Z. Li, S.-Y. Lee, *Adv. Funct. Mater.*, 2022, **32**, 2108798; (i) H. Hu, X. Lou, C. Li, X. Hu, T. Li, Q. Chen, M. Shen, B. Hu, *New J. Chem.*, 2016, **40**, 9746–9752.

14 Z. Luo, L. Liu, J. Ning, K. Lei, Y. Lu, F. Li, J. Chen, *Angew. Chem. Int. Ed.*, 2018, **57** ,9443–9446.

15 J. Zhao, T. Kang, Y. Chu, P. Chen, F. Jin, Y. Shen, L. Chen, *Nano Res.*, 2019, **12**, 1355–1360.

16 H. Wu, Q. Meng, Q. Yang, M. Zhang, K. Lu, Z. Wei, *Adv. Mater.*, 2015, **27**, 6504–6510.

17 C. Wua, M. Hua, X. Yana, G. Shanc, J. Liua, J. Yang, *Energy Stor. Mater.*, 2021, **36**, 347–354

18 H. Zhang, W. Sun, X. Chen, Y. Wang, *ACS Nano*, 2019, **13**, 14252–14261.

19 Z. Song, Y. Qian, T. Zhang, M. Otani, H. Zhou, *Adv. Sci.*, 2015, **2**, 1500124.

20 Y. Liang, P. Zhang, S. Yang, Z. Tao, J. Chen, *Adv. Energy Mater.*, 2013, **3**, 600–605.

21 D. Wilkinson, M. Bhosale, M. Amores, G. Naresh, S. A. Cussen, G. Cooke, *ACS Appl. Energy Mater*., 2021, **4**, 12084−12090
22 Y. Liang, Z. Chen, Y. Jing, Y. Rong, A. Facchetti, Y. Yao, *J. Am. Chem. Soc.*, 2015, **137**, 4956−4959.

